Insights about inductively coupled plasma optical emission spectroscopy interferences of major rare earth elements in complex e-waste feeds

Ajay B. Patil [a,b,*], Mohamed Tarik [a,*], Albert J. Schuler [a], Laura Torrent [a], Rudolf P.W.J. Struis [a,b], Christian Ludwig [a,b]

[a] Chemical Processes and Materials Research Group, Laboratory for Bioenergy and Catalysis, Paul Scherrer Institute, Forschungsstrasse 111, CH-5232 Villigen PSI, Switzerland
[b] École Polytechnique Fédérale de Lausanne (EPFL), ENAC IIE GR-LUD, CH-1015 Lausanne, Switzerland

ABSTRACT

The advent of rare earth elements (REEs) with optoelectronic properties has shifted the technology paradigm from digital to a smart and hybrid world. Their substantial uses also resulted in a large piling up of e-waste. Therefore, e-waste is now a lucrative recycling target for the recovery of such critical raw materials. Their recycling from e-waste is often challenged by dilute metal concentration, complex composition, and difficult chemical characterisation. Generally, the characterisation of e-waste involves elemental determination techniques, such as inductively coupled plasma optical emission spectroscopy (ICP-OES) or inductively coupled plasma mass spectrometry (ICP-MS). ICP-OES is attractive for a recycling or research sector because it has a higher matrix tolerance and lower cost than ICP-MS. In this work, the intensity at 445 line positions measured by an ICP-OES instrument was compiled in a 2D diagram to map interferences by 27 prominent lines from 9 REEs. The second diagram shows the impact at 230 neighbouring line positions measured in each of, in total, 17 (i.e., 9 REEs and 8 non-REEs) single-standard solutions in terms of the concentration of the element type affected. The spectral interference correction algorithm proposed here had been developed by us for a recycling process to obtain pure Y, Eu, and Tb from fluorescent powder (FP) in spent lamps. The ICP-OES analysis and spectral interference correction approach presented here can be applied to any element and e-waste type. To underline this, the paper gives examples for elements in dissolved FP and surrogate NdFeB magnet samples.

1. Introduction

Rare-earth elements (REEs) designate a group of 17 metals (Sc, Y, La-Lu) comprising most of the major electronics we use nowadays [1,2]. Therefore, the composition of REEs contains 15 lanthanides along with Sc and Y. They outrivalled the performance and features of conventional transition metal-based technologies. Their remarkable properties are due to a large number of unpaired electrons in their 4f subshells [3–5], imparting them with impressive optical, magnetic, or electronic properties and making them unique raw materials [1,6]. However, being part of electronic appliances, REEs are reaching municipal e-waste streams, which is one of the fastest-growing wastes worldwide with more than 10% annual growth [7–9]. Therefore, e-waste has been considered as a secondary resource for critical REEs by using appropriate recycling technologies [10–19], which is often challenging due to low

concentrations of different REEs, complex e-waste matrices, and the need for elaborate analytical techniques to facilitate detailed chemical characterisations [9,20–23]. REEs' high optical sensitivity and spectral interferences among each other and between other element types complicate their spectral properties [24]. Elemental techniques such as inductively coupled plasma optical emission spectroscopy (ICP-OES) and inductively coupled plasma mass spectrometry (ICP-MS) are widely used tools used for REEs analysis. They are implemented along with total reflection X-ray fluorescence spectrometry and radiotracer-based techniques such as neutron activation analysis depending on the scope of application [25–29]. The established interference correction protocols such as blank corrections and using primary standards are not suitable for complex and unknown matrix in e-wastes. Also conventional interference correction approaches lacks the post-processing correction possibilities. ICP-OES is generally applied due to higher matrix tolerance

---

and fewer costs than ICP-MS, which are indispensable criteria in recycling and waste management. In e-waste analysis, the presence of different REEs can lead to signal interferences between them and with adjacent emission lines from other elements. ICP-MS provides lower limits of detection than ICP-OES and it is becoming a robust technique, however it has less matrix tolerance and appropriate dilutions are required. Interference is the process that affects elemental interaction with light or gas phase atomization in atomic spectroscopy. This effect changes/alters the signal of the analyte during its measurement due to influence of coexisting elements Interferences are mainly divided into types such as spectral interferences and chemical interferences. Spectral interferences are caused due to the emission of contaminants in a similar wavelength region of the analyte. Chemical interferences are caused due to inefficient solubility and solids formation. It makes the chemical characterisation of such matrices challenging because it can lead to erroneous quantification results or improper impurity profiling [29–36]. Recent literature underlined the need for interference rectification with plasma-based analytical techniques to make the results more reliable [31,37], but also expandable to other waste types or feedstocks [32,33]. This is particularly needed in circular economy based process developments. Because in available literature, matrix related effects for e-wastes are unavailable, interference mapping is done only in pure REE analyte environments and there is no possibility of post-analytical corrections of interferences which is very important for the destructive analytical technique like ICP-OES. These aspects are precisely addressed by current paper.

For REEs determination with ICP-OES, detailed spectral interference patterns had been elaborated in the form of model tables by Boumans et al. and Daskalova et al. in several independent articles published about 20–30 years ago [33–35]. Although focusing on pure REEs samples only, the results can be used to identify and avoid potential spectral interferences. With e-waste samples, reports are rare [30]. Understanding spectral behaviour, peak evolution and broadening by instrumental and matrix effects are important aspects of analytics [36–41].

The primary objective of this study is to provide a methodology based on an algorithm and interference mapping, which can give a comprehensive picture of the spectral interference possibilities in the characterisation of complex e-waste. Mutual spectral interferences can be caused by the valuable metals targeted in a recycling process as well as by impurities co-present in the matrix. It can also be caused by other elements/impurities that need to be quantified for quality control purposes of the recycled products. REEs and REE containing feedstocks are traded on a trace metal basis in the market. It is thus essential to avoid misleading characterisation, process development, and quality control with the economically restricted e-waste management field. The major shortcoming with conventional ICP-OES instrument software is that it is based on existing literature or simulations with limitation to deal with complex and multi-element interferences, whereas e-waste management and recycling of strategic elements is a growing research field with known and new components in highly intricate matrices that were hardly thoroughly characterized before. Hence, the database and listed potential spectral interference effects are not comprehensive enough to accommodate these special classes of complex mixtures. The present work gives an advantage over highly sophisticated and labour-intensive spectral interference detection techniques (such as peak profile measurements) and over conventional software that is not suited for complex e-waste systems in that it does not allow rectification and correction in the post-processing of the measured data.

The present work evaluates qualitatively and quantitatively the ICP-OES spectral interferences for 445 and 230 spectral lines to provide a methodology based on an algorithm and interference mapping, which can help to identify and correct the quantification of REEs and their impurities in complex e-waste samples. In addition, the developed methodology is applied to quantify REEs in fluorescent powder (FP) from spent lamps and surrogate NdFeB magnet samples.

2. Materials and methods

2.1. Reagents and instrumentation

In this work, 17 single-element 10 mg/L standard solutions (9 REEs & 8 non-REEs), viz., Al, Ca, Ce, Dy, Eu, Gd, Fe, In, Mn, Na, Nd, La, Sc, Tb, Y, Zn, and Zr were purchased from Bernd Kraft GmbH, Fluka Analytical, Germany and Merck. Switzerland. Two multi-element standard solutions were also employed. The first one was from Fluka Analytical, Switzerland and it contained 10 mg/L of 16 REEs: Sc, Y, La, Ce, Pr, Nd, Sm, Eu, Gd, Tb, Dy, Ho, Er, Tm, Yb, and Lu. The second one was from Bern Kraft GmbH, Germany and it comprised 30 elements: 2.5 mg/L of Ag, 50 mg/L of P and K; and 10 mg/L of Al, As, B, Ba, Be, Ca, Cd, Co, Cr, Cu, Fe, Hg, Li, Mg, Mn, Mo, Na, Ni, Pb, Sb, Se, Si, Sn, Sr, Tl, V, and Zn. The standards were diluted with 1% nitric acid, which was prepared with analytical grade trace select quality nitric acid (HNO_3, 65%, Sigma Aldrich, Switzerland) and high purity water from a Milli-Q purification system (Sartorius, Germany). An ICP-OES Ciros and Arcos Vision (Spectro Analytical Instruments, Germany) with a spectrum range from 125 nm to 770 nm were used in the present work, together with the ICP Analyzer Pro Software. With this instrument, 445 and 230 optical emission lines were measured and quantified, respectively. After measuring the blank solution (1% HNO_3), each sample was recorded and the ICP-OES was cleaned after that by flushing with a fresh blank solution until reaching the same background level as before the sample measurement. The instrumental characteristics and measurement conditions are specified in Table S1 from the Electronic Supporting data (Appendix).

The Origin 2018 software was used for data analysis and characterisation of three REEs line profiles for purposes of discussion and presentation.

2.2. Preparation and analysis procedure of e-waste materials

E-waste recycling processes with spent lamps involve shredding, segregation, and digestion of the recovered FP. The hard lanthanides and actinides need to be dissolved in an acid medium for the ease of analysis in solution conditions and wet chemical steps for purification purposes for the targeted REEs [9,23,41]. In FP waste, >50 REEs and non-REEs are present in a complex matrix due to the different phosphors: HALO $((Sr,Ca)_{10}(PO_4)_6(Cl,F)_2:Sb^{3+}, Mn^{2+})$, YOX $(Y_2O_3:Eu^{3+})$, LAP $(LaPO_4:Tb, Ce)$ and BAM $(BaMgAl_{10}O_{17}:Eu^{2+})$, and other components introduced by the shredding. BLUBOX Trading AG, Switzerland provided the shredded FP e-waste samples. A half milligram of the FP sample was dissolved in 10 mL 1% HNO_3. The real e-waste FP sample was inorganic and soluble in HNO_3. The sample was centrifuged before ICP measurement and no apparent organic/insoluble matter was observed. The detailed composition of the FP waste determined by ICP-OES is shown in Table S2 (see Appendix) and was determined in the frame of a patent application [19,23]. All samples mentioned above were used to understand the manifold of possible spectral interferences in the analysis of FP e-waste.

In addition, the developed method was applied to other e-waste samples to demonstrate it can be used for other elements and types of e-wastes. Permanent magnet-like samples were studied for Nd and Dy in the following three cases: (1) 50 μL 0.01 M $Nd(NO_3)_3$ + 50 μL 0.01 M Dy $(NO_3)_3$ in 10 mL 1% HNO_3; (2) 50 μL 0.01 M $Nd(NO_3)_3$ + 10 μL of 90% $Tb_2(SO_4)_3$-enriched FP solution as described by Patil et al. [9,19,23], together with 10 mL 1% HNO_3. The $Tb_2(SO_4)_3$-enriched FP solution is hereafter referred to as Tb(FP)*; and (3) 50 μL 0.01 M $Dy(NO_3)_3$ + 10 μL Tb(FP)* in 10 mL 1% HNO_3.

For the quantification of the analytes, calibration solutions with concentrations from 0 to 10 mg/L were prepared using single- and multi-element standards (Section 2.1).

3. Results and discussion

3.1. Peak profile of measured spectral lines

To develop the algorithm and interference mapping, we focused on 3 REEs that are present in FP. With FP waste, arguably Y, Eu, and Tb are the REEs with high recycling potential. Therefore, we kept the major focus on these 3 elements with high commercial recycling prospects. Other than this rare earth metals, such as La, Ce, and Gd, are also present in the FP e-waste. To understand how much a defined optical line is quantitatively contributing to adjacent lines, its profile should be precisely known. Therefore, shapes of three spectral lines were investigated: Eu 381.964 nm, Tb 350.917 nm and Y 324.228 nm. The three lines were chosen with respect to the presence of these metals in FP e-waste, as aforementioned. For the used ICP-OES system, the observed lines of other REEs and non-REEs seem to have a similar profile. The signals of these three lines were acquired during the measurement of the corresponding single-element standard solutions (10 mg/L). Each line profile was fitted iteratively by a combination of the following Gaussian and Lorentzian distributions (Eqs. (1)–(3)), where the parameters are defined as λ: wavelength, λ_0: central position ("mean") of the distribution, I_{max}: distribution intensity maximum in counts per second (cps) at $\lambda = \lambda_0$, σ^2: variance of the Gaussian distribution, γ: the half-width at half-maximum, and α: fitting parameter ($0 \leq \alpha \leq 1$).

$$F(\lambda) = \alpha\, G(\lambda) + (1 - \alpha)\, L(\lambda) \quad \text{(Distribution function used)} \tag{1}$$

$$G(\lambda) = I_{max}\, e^{-\frac{(\lambda - \lambda_0)^2}{2\sigma^2}} \quad \text{(Gaussian distribution)} \tag{2}$$

$$L(\lambda) = \frac{I_{max}}{1 + \left(\frac{\lambda - \lambda_0}{\gamma}\right)^2} \quad \text{(Lorentzian distribution)} \tag{3}$$

With Eq. (1), the two distributions have the same λ_0, same scale parameter ($\sigma = \gamma$), and same I_{max}. The λ_0 and the I_{max} are set equal to the λ and I_{max}, respectively. The scale parameter ($\sigma = \gamma$) and the parameter α were iteratively changed to achieve the best result on a sum of least-squares basis. Table 1 summarises the distribution and fitting parameters. The contribution of one of these lines at a wavelength difference $\Delta\lambda$ away from the λ_0 can be calculated easily using Eqs. (1)–(3) and the appropriate parameters (Table 1) at $\lambda_x = \lambda_0 + \Delta\lambda$. Therefore, Eqs. (1)–(3) helped in the peak profiling and were used to deduce such peak contributions of other specific REE wavelengths on the line with wavelength difference $\Delta\lambda$. In Table 1, an example of the contribution with each profile at $\Delta\lambda = +10$ pm is shown.

As can be shown in Table 1, the contribution of an optical emission line to neighbouring wavelengths depends strongly on the sensitivity (maximum intensity) and the shape of its line. The scale parameter value for the Gaussian and Lorentzian functions were found by us to be the same for all lines ($\alpha = 0.7$). However, the profile of each distribution function of a given line can vary due to different $\sigma = \gamma$ values. Therefore, the line Eu 381.964 nm has a higher interference potential ($\sigma = \gamma = 9.8$ pm), while that of Y 324.228 nm has a lower interference contribution to adjacent lines ($\sigma = \gamma = 4.4$ pm). The ratio of the maximum intensity and the intensity at a wavelength of 10 pm apart in the case of the Eu line is 0.56 and in the case of Y is only 0.10.

Table 1
Fitting parameters for the three measured spectral lines (see text for the definition of the parameters and quantities).

Line	λ_0 (nm)	$\sigma = \gamma$ (nm)	I_{max} (cps)	α	I at $\lambda_x = \lambda_0 + 10$ pm (cps)
Eu	381.964	0.0098	8.60E+06	0.7	4.84E+06
Tb	350.919	0.0076	8.70E+05	0.7	3.52E+05
Y	324.229	0.0044	3.55E+06	0.7	3.49E+05

3.2. Interference map for REEs recommended wavelengths

In total, 27 lines recommended by the ICP-OES software were chosen for 9 REEs. The intensity of each recommended line was determined in the corresponding 10 mg/L single-REE standard solutions, together with the intensities at 445 adjacent line positions from 17 other elements (not present with any of the 9 single-REE standards). The net intensity measured at each line position was calculated by subtracting the raw intensity of the blank sample (1% HNO_3 solution) measured at the same wavelength. In Fig. 1, the 27 recommended lines are indicated on the x-axis. The wavelength difference, $\Delta\lambda$, between a recommended and an adjacent line position is shown on the y-axis in three different plots, covering, in total, an interval between -100 pm to $+100$ pm around a given recommended line positioned at $\Delta\lambda = 0$, and with an increment of 1 pm for purposes of distinguishability (Fig. 1). On a practical level, however, the band-pass registered by a single pixel for most of the commercial ICP-OES instruments varies between about 5–10 pm, depending on the wavelength. In Fig. 1, the net cps intensity (blank-corrected) is indicated by the colour of the rectangle that is defined by the logarithmic colour scale. Table S3 shown in the ESI allows identifying the element at a given $\Delta\lambda$ distance away from a given REE recommended line (indicated at the top). Table S3 (from Appendix) is presented for illustrative purposes and without any claim to comprehensiveness. The lines rectified and corrected by us for the spectral interferences are from the National Institute of Standards and Technology (NIST) list and the Spectro ICP-OES database.

As can be inferred from Fig. 1, when $\Delta\lambda$ is increasing, the intensity is generally decreasing by about one order of magnitude for each ~30 pm. REE lines (x-axis) with intensities $<10^6$ cps mainly affect adjacent lines located within the interval $\Delta\lambda = \pm 30$ pm. The profile of the measured intensities at wavelengths positioned equidistant below ($\Delta\lambda < 0$) and above ($\Delta\lambda > 0$) the recommended REE spectral peak position is symmetric with many adjacent line positions. It means that this interference pattern is caused most probably only by the measured REE wavelength at $\Delta\lambda = 0$. The presence of other wavelengths from the same REE leads to an asymmetrical interference profile. Knowing the matrix content of a given sample and using Fig. 1 and Table S3 (see Appendix), a first selection of "appropriate" REE lines can be made. For example, by measuring the 10 mg/L Eu single standard solution, the Eu 381.967 nm line (shown on the x-axis of Fig. 1) was found capable of affecting another recommended line at $\lambda = 381.978$ nm. The latter line position lays above the Eu 381.967 nm line. In Fig. 1, the wavelength difference of $\Delta\lambda = +0.011$ nm ($=381.978–381.967$) is indicated on the y-axis. From Table S3 (see Appendix), it follows that the last-mentioned line belongs to the element Molybdenum (Mo). The number of REE lines and adjacent wavelength positions is neither bound nor limited to those shown here. They were chosen for demonstration purposes and aimed at different elements in real complex matrices from different e-waste types. The large selection presented here is therefore not a prerequisite with specific e-waste or every single or multi-element standard solution. The presented approach could be applied to a set of elements in the matrix and chosen emission lines as demonstrated here.

With Eu, the emissions at the three selected wavelengths (Fig. 1) are high and the intensities are also still substantial at neighbouring line positions from other elements. For example, following the intensities (Fig. 1) of the Eu 381.967 nm line and by the way of example listed elements for FP and NdFeB magnets at adjacent line positions (Table S3 (Appendix)), it appeared that the mentioned Eu line can hypothetically interfere with different elements with the following order of the degree of the interference effect ("order"): Cr > Mo > Fe > S > Hf > V > Sc > Sc (2nd line) > Nb > Pr > Cl > Ru > Ce > Nd. The impact of this bright Eu line extends over a quite large wavelength interval ($\Delta\lambda = \pm 66$ pm). Due to the high matrix complexity, but irrespective of whether the element is the analyte or the interferent, signal interferences between elements can affect the characterisation, processing, and quality control of recycled products, as well as, lead to false profiling and quantification of matrix
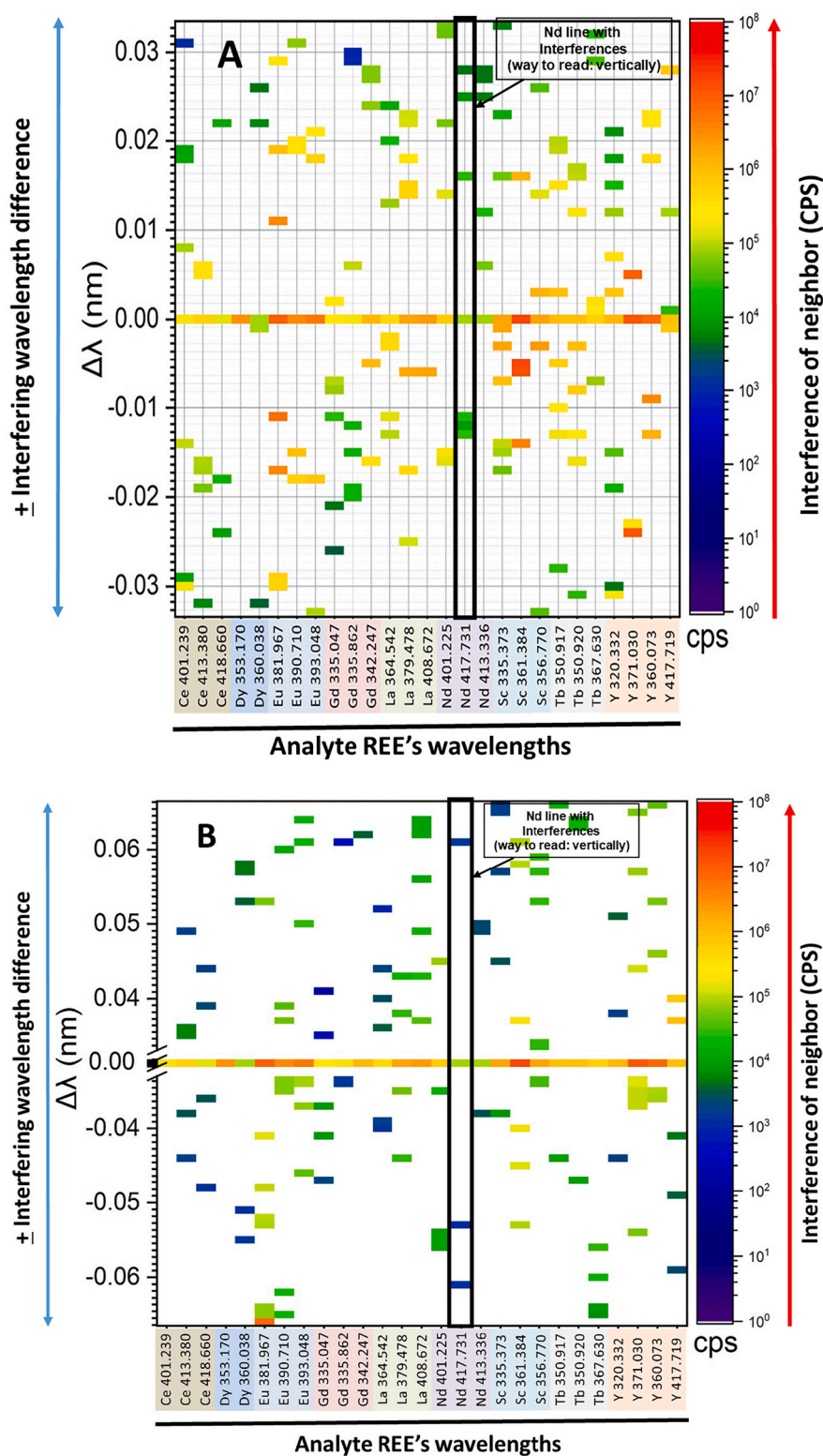
Fig. 1. The intensity of some recommended REE lines (x-axis) measured in 10 mg/L single-REE standards is indicated on the y-axis under $\Delta\lambda = 0$ nm. The intensity of the REEs lines at adjacent line positions for other elements with $\Delta\lambda$ (nm) between -0.033 and $+ 0.033$ nm (A); the interferences observed with $\Delta\lambda$ between -0.033 to -0.066 and $+ 0.033$ to $+0.066$ nm (B); the interferences observed with $\Delta\lambda$ and between -0.066 to -0.100 and $+ 0.066$ to $+0.100$ nm (C). Way to read the Figure has been explained with vertical black box with respect to Nd line as an example.

impurities. For example, at $\Delta\lambda = -48$ pm away from the Eu 381.967 nm line, an intensity of 1.07×10^5 cps was measured with the 10 mg/L single-element Eu standard. The intensity value was also calculated by using Eq. (1) and Table 1. On the other hand, measuring the multi-REE standard solution also containing 10 mg/L Eu, the intensity at $\Delta\lambda = -48$ pm was 1.57×10^5, which is much larger than determined with the
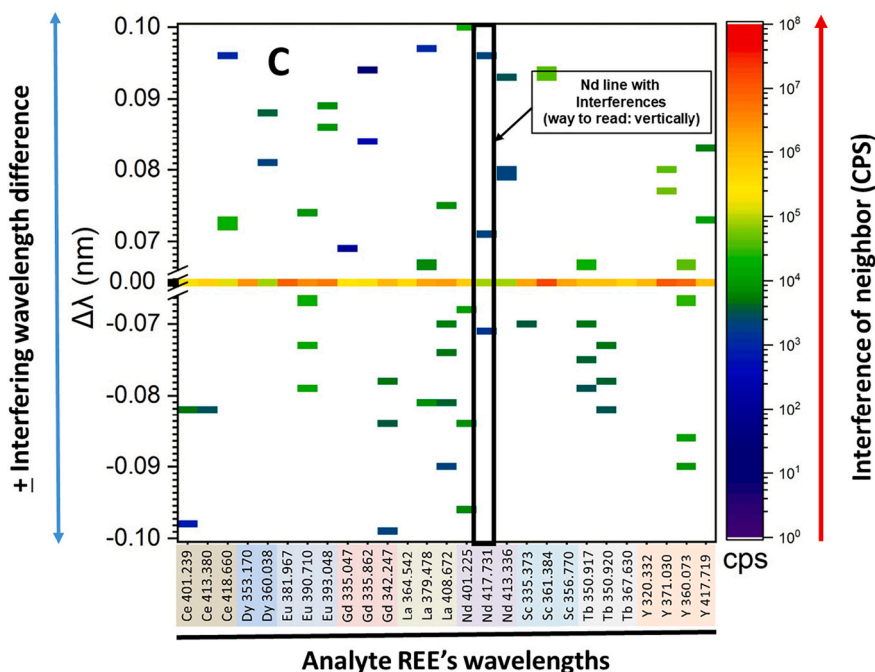
Fig. 1. (*continued*).

single Eu standard, suggesting the co-presence of another element. This was also apparent by the asymmetric intensity distribution profile measured for negative and positive Δλ's (not shown here). Following Table S3 (see Appendix), the line in question could be that of Sc at 381.919 nm, and Sc was indeed a co-element with the multi-REE standard solution.

The emission lines of the Y can interfere with the lines of other elements (when present). For example, the Y 360.073 nm line could affect the following elements in the order: Rb > Nd > Ho > Gd > Dy > Cl > Zr > Mn > F > Sc > S > Hf > Er. The Tb 350.917 nm and Tb 350.920 nm lines have another interference order pattern: Fe > Mn > Zr > Au > Cl > Ho > Ti > Co > W > Lu > Er. The profile of these two Tb peaks is described reasonably well by one hybrid distribution function with $\lambda_0 = 350.919$ nm (Table 1) because they are only 3 pm apart. For example, the measured and the calculated intensities using the hybrid distribution function at the Ho 350.937 nm line position, which is 17 pm away from Tb 350.920 nm and 20 pm from Tb 350.917 nm, are 9.63×10^4 cps and 9.77×10^4 cps, respectively. With increasing Δλ the probability of interference can be seen from Fig. 1 (Δλ = 1a < 1b < 1c; interference = 1a > 1b > 1c). Generally, finding a 100% interference-free emission line for a complex matrix is difficult. However, with the help of the plots shown in Fig. 1, one could make a selection of appropriate lines for the analytes based on high line sensitivity (as it is done with conventional ICP-OES analysis software) and here together for the lowest interference impact for the co-present elements.

3.3. Relating the interfering signal intensity to the concentration of the analyte affected

In ICP-OES analysis, the 'blank' is a solution with the same (or similar) matrix. Here, the standard, the blank, and the other samples were all prepared in 1% HNO_3. From the 445 available wavelengths, 230-emission line positions for, in total, 17 different elements were measured in each of the 17 corresponding 10 mg/L single-element standard solutions. The blank corrected intensity values were quantified in terms of the concentration following the single-element standardisation of the affected analyte in question. In Fig. 2, the concentration is given as a colour defined on the logarithmic scale shown. In contrast, each standard line has the colour for 10 mg/L in line with the

concentration with the single-element standards used.

The interference impact depends on the line sensitivity ("peak signal per concentration unit") of the analyte and the interferent in question. If the analyte line is not very sensitive, already a small signal contribution from the interferent can lead to a much higher concentration than in the absence of the interferent. For example, the presence of Eu in multi-element standards or samples can lead to substantial interferences with the much less sensitive lines of Ce, Fe, Sc, and Y, while Tb may affect other lines, including those of Ce, Dy, Eu, Sc, and Zr. Furthermore, Y interferes at different wavelengths with Dy, Gd, Mn, Nd, Sc, and Zr. Misleading results can e.g. also follow when the probed analyte is not present in the interferent-containing sample.

The 17 single-element standards were also used to quantify the signal intensities measured in a 16 REE-containing multi-standard solution (labelled as "REE" in Fig. 2), comprising 10 mg/L of each of these REEs, and in a multi-standard solution comprising 30 non-REEs (referred as "Multi" in Fig. 2). The composition of these standards is given in Section 2.1. With several REE lines, the "REE" multi-element solution rendered higher elemental concentration values when compared with the corresponding single-REE standards. Thus, a quantification procedure of unknown samples using the affected lines and a REE multi-standard solution would result in under- or overestimated concentration values of the elements of interest, depending on the matrix content and condition in these samples. Similar trends are discernible in Fig. 2 with the multi-non REE-element solution when using the corresponding single non-REE standards.

3.4. Quantification of elements in dissolved e-waste samples

Recently, several research groups were focusing on developing a technology to recycle critical rare earths, such as Y, Eu, Gd, Tb, Ce, and La from FP e-waste. However, this waste contains a complex matrix comprising different classes of elements in the periodic table, except for noble gases and radioactive actinides [8,11,15,19]. Y is the most abundant REE metal in FP waste [9,23]. Our recycling process aims to obtain pure Y, Eu, and Tb from FP e-waste [19,23]. During the entire process, the developed analytical ICP-OES method was used to quantify the different REEs and non-REEs with the original FP up to the pure end products. Fig. 3a–e show interference examples measured in the multi-
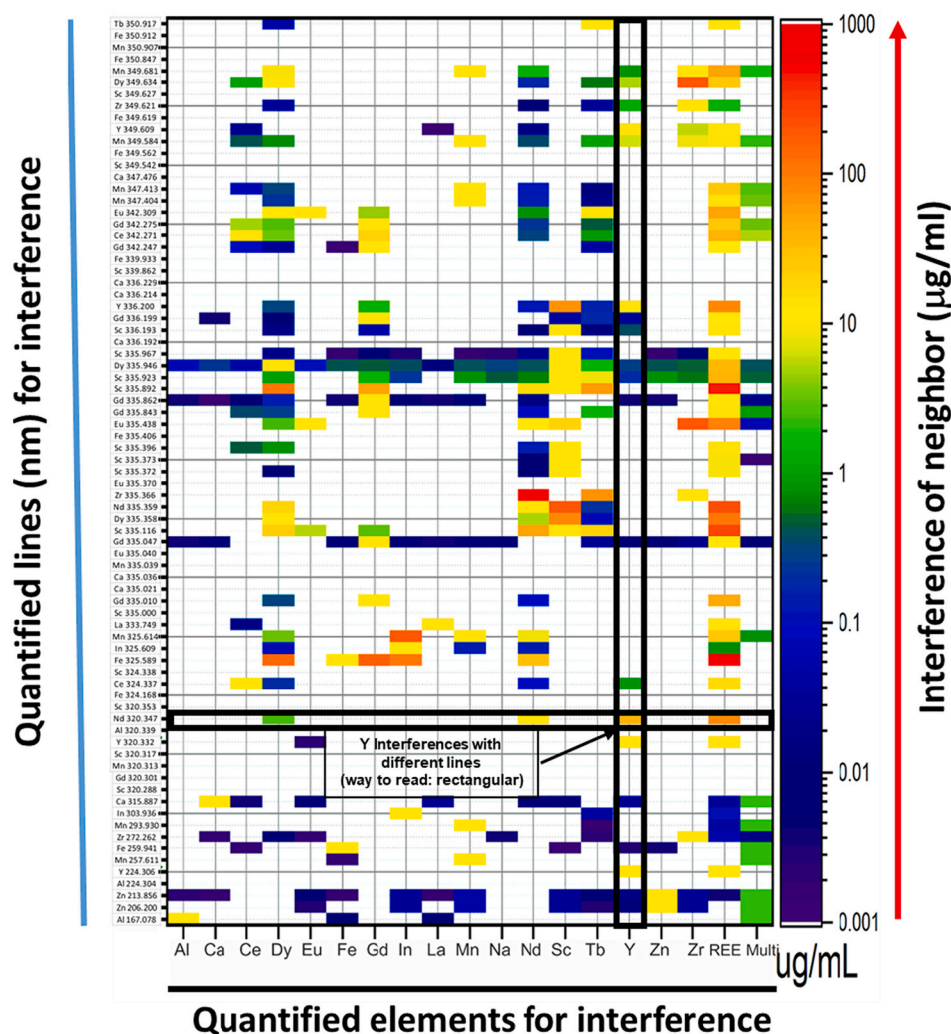
Fig. 2. Quantification of signal interferences from 17 elements (x-axis) that were measured in single-element, multi-REE ("REE"), and multi-non-REE ("Multi") standard solutions at 230 line positions shown on the y-axis for wavelengths between λ = 160 nm–590 nm. Way to read the Figure has been explained with rectangular black boxes with respect to Y element as an example.

REE standard ("REE") together with the same lines measured in the respective single-element standards. Fig. 3f shows the overlay of lines of Zr and Y (349.609 nm) from their standards.

With FP, an important and valuable REE is Eu with the red phosphor. The Eu 390.710 nm line can interfere with the lines of Ce and Sc (Fig. 3a). Interferences between Sc, Y, and Gd are also thinkable (Fig. 3b). Interferences between Ce and Gd can occur for their lines listed at 342.271 and 342.247 nm, respectively (Fig. 3c). Due to the most sensitive line chosen for Y, we faced serious interference and the false presence of Nd content in our samples (Fig. 3d). As can be seen in Fig. 3e, Tb and Dy lines show that can interfere with each other, consequently affecting their measurement in FP. The FP from shredded e-waste does usually also contain a mixture of S, Si, Pb, Zr, Cr, and other impurities, including In (with LCD panels), V, and As, that could also give misleading counts with the emission lines of the REEs, and vice versa. An illustrative example is shown for Y and Zr in Fig. 3f. FP waste also contains considerable amounts of alkaline earth metals, for instance, Ca as a part of the HALO ($(Sr, Ca)_{10}(PO_4)_6(Cl,F)_2$:$Sb^{3+}$,$Mn^{2+}$) phosphor. In the analysis of REEs such as Gd and Ce, also interferences can be expected due to the presence of the Ca line at 393.366 nm (not shown here). In summary, some insights gained about interferences that can occur with FP e-waste containing solutions: the analyte and interferent are chosen arbitrarily and can also apply the other way round.

Another e-waste of interest could be that of NdFeB magnets. In commercial sintered NdFeB magnets, Nd is usually partially substituted by other REEs including Pr, Dy and Tb, in the co-presence of other transition metals, such as Fe, Co, Al, etc. [4,5,8,42]. After inspecting Table S3 (see Appendix), several interferences between these elements become apparent, and one case for Dy and Tb is shown in Fig. 3e. In the ideal case, interferences caused by the REEs present in NdFeB magnets at emission lines of other REEs from other e-waste, such as Y and Tb from FP, are usually absent in magnet e-waste matrices, and vice versa. And, the same goes for the other, unwanted, rare earth and transition metal impurities. However, in case an element is not present with a sample but included with the measuring protocol as a quality control requirement, it can behave as a potential interferent as it can be observed in Fig. 3d (interference between Y at 417.754 nm by Nd). As a consequence, this may lead to erroneous element profiling and quantification result for the alleged interference. Such misinterpretations were our main reasons for carrying out this systematic study and designing a general protocol to avoid them (if possible) or to correct the quantification result for a true interference affected analyte because this is needed particularly with ICP-OES analysis in complex e-waste recycling process development and product quantification work.
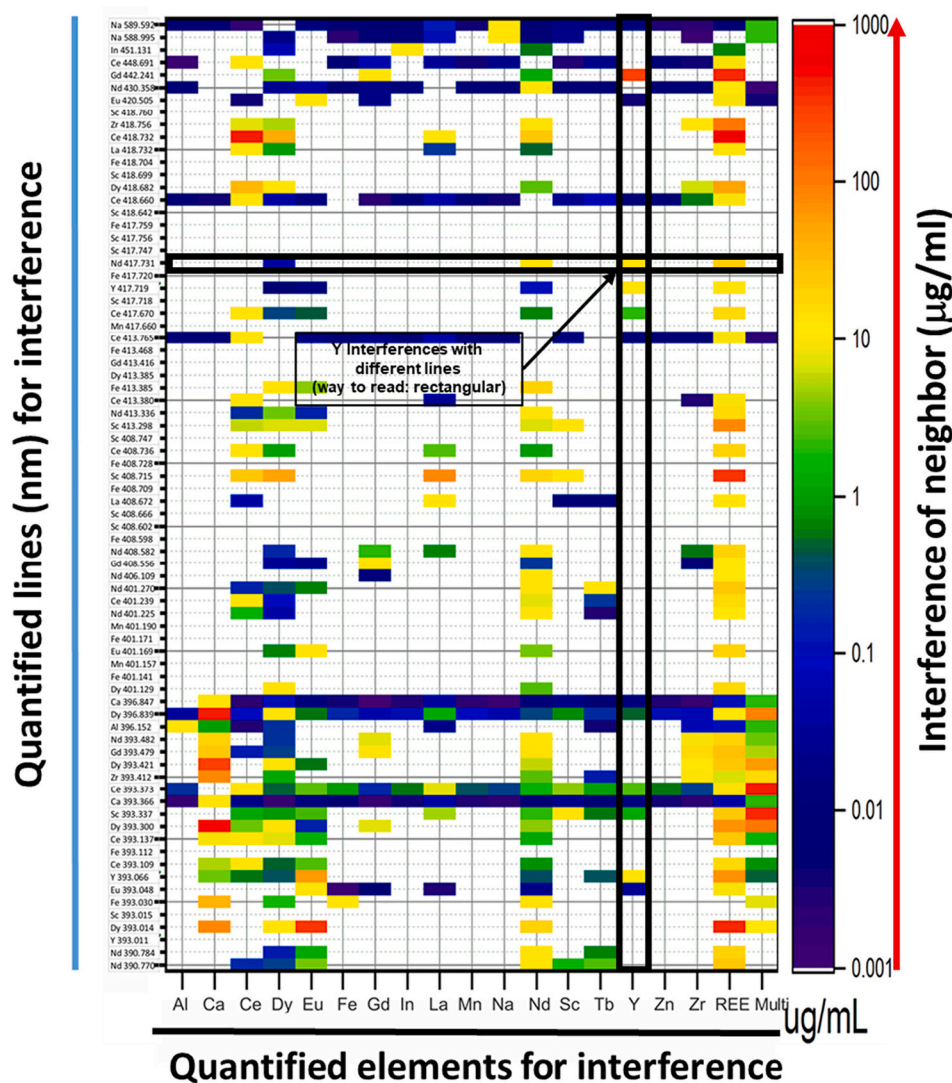
Fig. 2. (*continued*).

3.5. Interference correction procedure

In literature, conventional methods such as blank corrections, surrogate matrix preparations and reference standards are used. However, it is very difficult to follow such methods in the case of the complex and unknown matrix of the e-wastes [21]. The complex composition of original (non-treated) FP e-waste after acid digestion results in substantial interferences for REEs analysis by ICP-OES, in particular by its major element Y and the less abundant elements, such as Eu, Tb, La, Ce, and Gd (Table S3 (Appendix)). The signal contribution by the interferent line can be corrected, and the analyte concentration can be quantified properly after that. The following example is given in general terms because the procedure is not restricted to any e-waste, analyte, interferent, recycling, processing, or production stage in particular. In addition, it can be applied to different matrices and elements as is demonstrated in this section. A net intensity $I_{A+B}^{x, sp}$ is measured in a sample ('sp') at wavelength λ_x. The value is the sum of the emission intensity by the analyte A and that of the interfering element B, such that $I_{A+B}^{x, sp} = I_A^{x, sp} + I_B^{x, sp}$. The net intensity, $I_B^{y, sp}$, of an interference-free (or negligibly influenced) line of the element B present in the sample is measured at wavelength λ_y. The ratio $\frac{I_B^{x, st}}{I_B^{y, st}} = \frac{I_B^{x, sp}}{I_B^{y, sp}} = \alpha_y^x$ can be calculated from the 10 mg/L single-element standard solutions ('st') for element B, so that $I_A^{x, sp} = I_{A+B}^{x, sp} - (\alpha_y^x * I_B^{y, sp})$. Table S4 (see Appendix) shows

some experimental α_y^x values derived in this work. The true concentration then follows from $I_A^{x, sp}$ and the experimental single-element calibration curve for element A at λ_x.

In Table 2, several examples are given to compare the quantification results for different elements as the analyte from three different quantification approaches: (1), using the multi-REE standard calibration. The resulting analyte concentration is shown under the column "Conc. 1". (2), using the single-element standard of the analyte without any correction after that. The result is given under "Conc. 2" and, (3), using the single-element standard of the analyte with the above-outlined interference correction algorithm. The result is listed under "Conc. 3". The samples shown in Table 2, which were analysed by ICP-OES, include a solution of digested FP e-waste ("FP"), the "Nd + Dy" and the "Dy+Nd" solution mixtures described in Section 2.2, and a Tb-enriched FP solution ("Tb(FP)*") that was achieved during the development of our FP recycling process [19,23]. It can be inferred from examples 1, 6, 7, and 8 (Table 2), that a real additional signal at the analyte line caused by another element leads to higher intensity (more counts) for a given analyte concentration with the REE multi-standard than with an equally concentrated single-analyte standard. Therefore, the analyte concentration value under "Conc. 1" is lower than the one under "Conc. 2". Following the interference corrected result under "Conc. 3", the inequality occurs irrespectively whether the analyte is present (examples 7,8) or absent (examples 1,6) with the sample under study. With
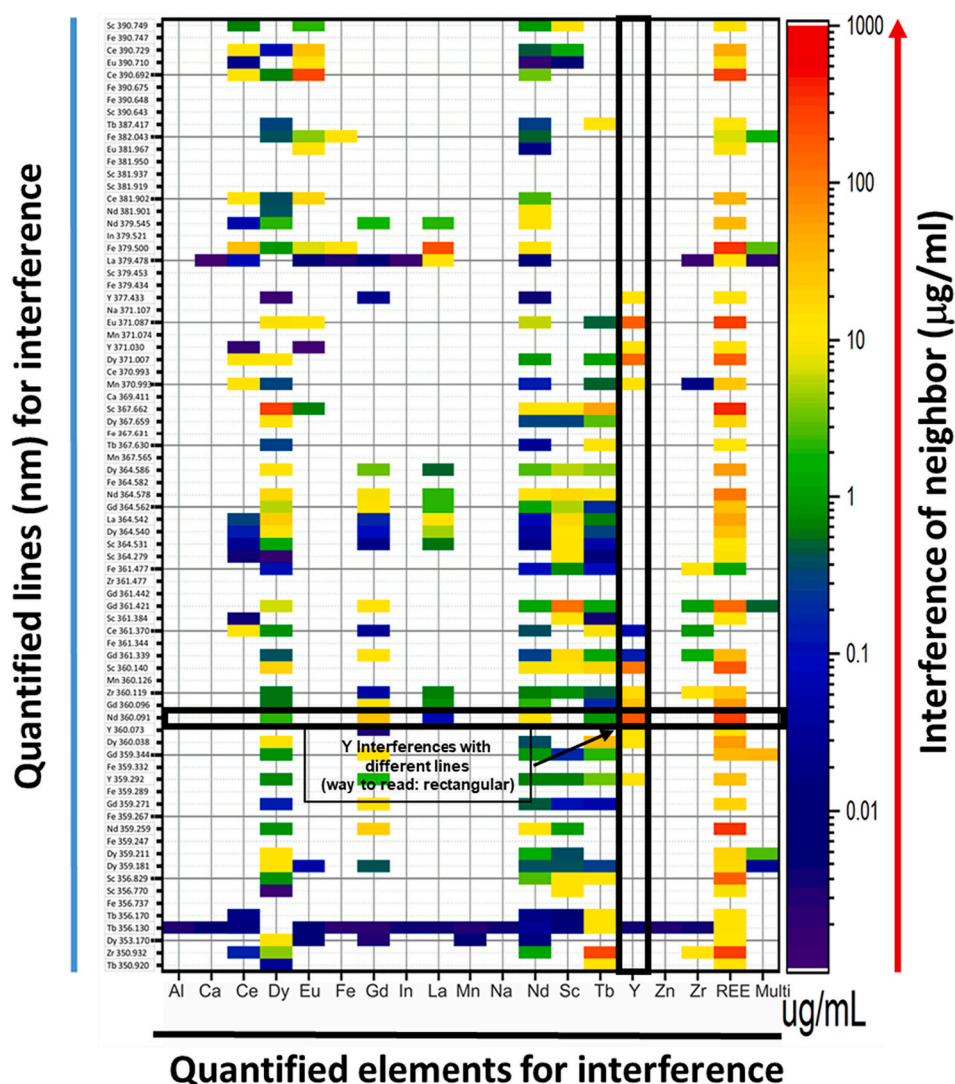
Fig. 2. (*continued*).

cases 2 and 4, on the other hand, the analyte concentration values changed hardly between the three approaches, because the alleged interference by Ce in case 2 is insignificant (this is also apparent by inspecting Fig. 3a more closely), and that of Zr in case 4 did not occur at all because Zr was absent in the FP sample. From the above examples, it is clear that in complex matrices, such as those from e-wastes, interference correction procedures are indispensable for correctly quantification of analytes with ICP-OES. The exact theoretical values of the metals are not known in complex e-waste mixtures due to variation between manufacturers and recycler's compositions. Therefore, e-waste analytics validation has a practical limitation. However, using our inference rectification and correction approach the value of "Conc. 3" in Table 2 is the closest to the actual one as the optical interferences are eliminated by our post-processing correction method. This is very well demonstrated with example 1 in Table 2, as the falsely detected Nd was factually absent in FP samples. Its alleged presence suggested in "Conc. 1" and "Conc. 2" is due to the bright Y line, which is a major REE in the FP sample.

The correction of the calculated concentrations was done by using the blank and the single standard concentrations of the two elements (analyte and interfering element) at different lines as described in the paper. The used intensity at an interfering line is measured and not calculated. Then, using the linear calibration for the element corresponding to this line, the actual interference can be directly quantified

(without knowing the entire profile of the line causing this interference). In general, for such an ICP-OES instrument, the relationship between the net intensity and the concentration is linear between 0 and 10 ppm. Therefore, our correction approach would be certainly useful independent of the analyte concentration.

The validation of the method and interference rectification in complex e-waste matrices is very difficult due to the unavailability of a reference standard or matrix. This is universal pain in the waste management process development and the analytics field. However, we tried to validate the achieved results in Table 2 by using ICPMS as an alternative. The concentrations found with the validation by ICPMS are shown in Table 2 as concentration 4. It can be seen that they are fairly closer to the corrected values for the ICP-OES interferences. Therefore, It is validated that concentration 3 (calculated concentration using single-element standards with interference correction applied after that) for Nd, Sc and Ce were < LOQ; (which is actual value). The limit of detection for the elements found in the studied e-waste matrix is shown in Table S5 (see Appendix). Although these metals are, absent in referred samples; they have to be analysed to characterize the e-waste, process steps and recycled metals fractions. Validation confirmed the effectiveness of our developed spectral interference correction method. It is worth mentioning that, the lines measured for all the elements of interest for e-waste characterisation for their REE content, are from an instrumental and NIIST database.
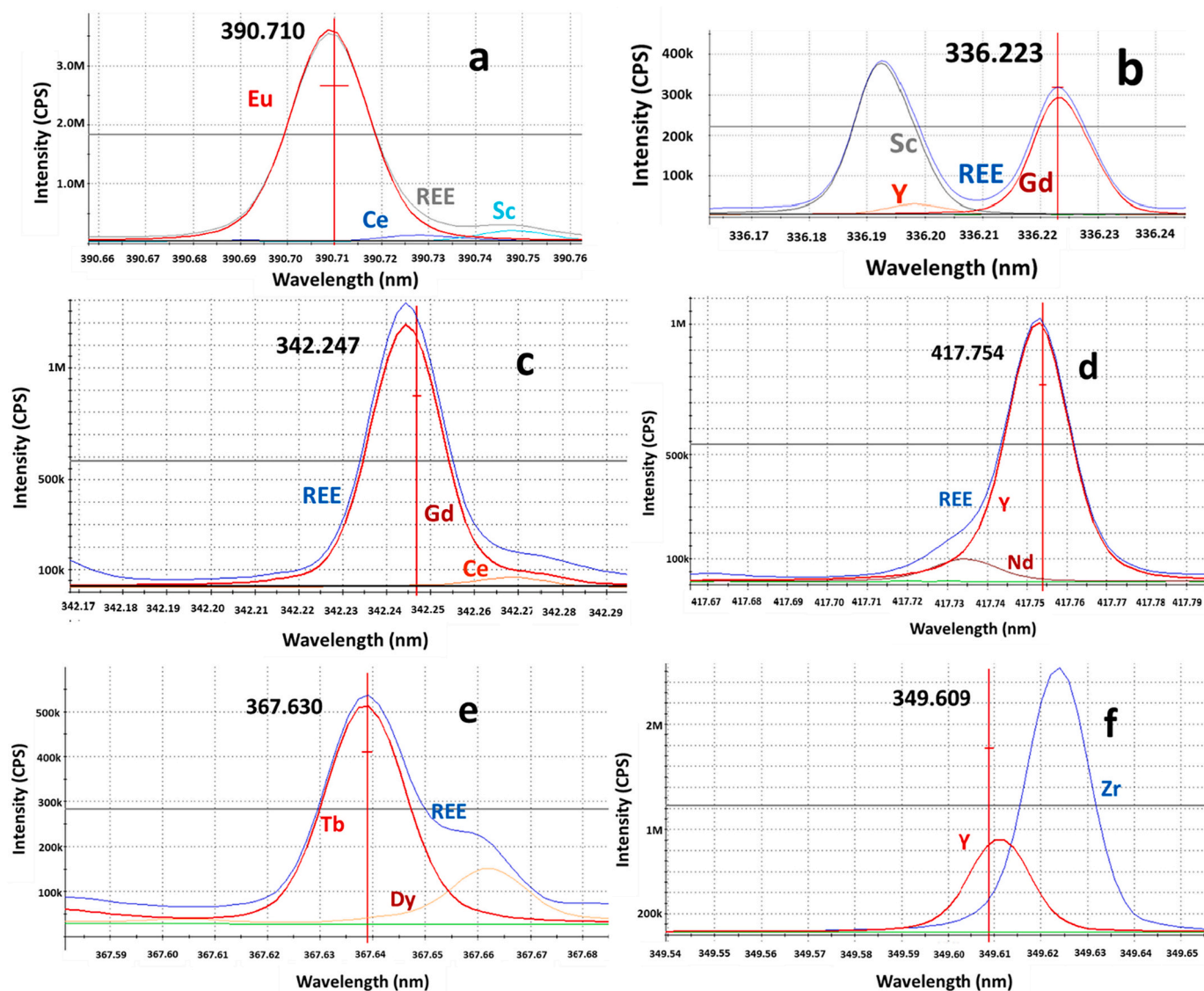
Fig. 3. Interference examples measured in the multi-REE standard ("REE"), together with lines from single-element standards (a–e). Representation of the overlay of the Y 349.609 nm line and the nearby Zr line from single-element standards (f). The name of the analyte and its line is in red.

Table 2

Examples of quantification using multi- or single-element standards with and without interference correction: Conc. 1 (µg/mL) = calculated concentration using a multi-element standard; Conc. 2 (µg/mL) = calculated concentration using single-element standards; Conc. 3 (µg/mL) = calculated concentration using single-element standards with interference correction applied after that; Conc. 4 (µg/mL) = determined concentration for the validation of corrected values.

Example	Sample	Analyte	Calibration line used	Interferent line	Line for correction	Correction factor	Conc. 1	Conc. 2	Conc. 3	Conc. 4[(d)]
		X	λ_x	$\lambda_m = \lambda_x + \Delta\lambda$	λ_y	α_y^x	µg/mL	µg/mL	µg/mL	µg/mL
1		Nd	Nd 417.731	Y 417.754	Y 371.030	137.5	5.76	12.46	<LOQ[(c)]	0.01
2		Eu	Eu 390.710	Ce 390.692	Ce 413.380	75.9	0.88	0.86	0.86	0.81
3	FP	Sc	Sc 336.193	Y 336.200	Y 371.030	864.4	0.025	0.025	<LOQ[(c)]	0.001
4		Y	Y 349.609	Zr 349.621	Zr 361.477	1.1	13.96	13.91	13.89	13.88
5		Zr	Zr 349.621	Y 349.609	Y 371.030	38.1	#[(b)]	3.30	1.53	0.049
6	Nd + Dy	Ce	Ce 401.239	Nd 401.225	Nd 413.336	0.5	3.03	4.61	<LOQ[(c)]	0.005
7	Dy +Tb(FP)* [(a)]	Ce	Ce 401.239	Nd 401.225	Nd 417.731	0.5	3.00	4.57	0.16	0.26
8		La	La 364.542	Dy 364.540	Dy 353.170	2.8	3.06	15.32	0.46	0.39

(a) Tb(FP)* = FP e-waste sample enriched in Tb (see references [19] and [23]); (b) # = Zr was not present in the multi-REE standard; (c) < LOQ: Concentration value lies below the experimental limit of quantification; (d) Concentrations determined by using the ICP-MS for method validation (uncertainty ±8%).

4. Conclusions

The simple method to correct the ICP-OES spectral interferences for REEs has been proposed and demonstrated with a real e-waste example.

The approach uses measured intensities of the analyte and interfering elements at different wavelengths and is independent of the analyte concentrations. It is also more effective than the calculated intensities with conventional instrument software or interference correction

protocols that are unable to handle the complex matrix like e-wastes. The method also provides the quantitative post-processing interference correction advantage.

Using ICP-OES as the analytical tool for the development or control of a recycling process for complex e-waste, misinterpretations due to the higher number of spectral interferences can mislead and delay its progress. This work provides substantial advantages for the e-waste management and recycling community in terms of a hands-on tool that is simple and efficient to use. Similar interference mapping and single-element standard-based correction procedures are also recommendable in future analytics and recycling process developments with different e-waste and metal feedstock.

CRediT authorship contribution statement

Ajay B. Patil: Conceptualization, Methodology, Investigation, Data curation, Writing – original draft, Writing – review & editing, Visualization, Funding acquisition. **Mohamed Tarik:** Conceptualization, Methodology, Investigation, Data curation, Writing – original draft, Writing – review & editing, Visualization. **Albert J. Schuler:** Methodology, Investigation, Resources. **Laura Torrent:** Data curation, Writing – review & editing. **Rudolf P.W.J. Struis:** Methodology, Writing – review & editing, Supervision. **Christian Ludwig:** Resources, Writing – review & editing, Supervision, Funding acquisition.

Declaration of Competing Interest

Authors declare that they have no competing interests to declare associated with work reported in the present manuscript.

Acknowledgements

Appendix A. Supplementary data

Supplementary data to this article can be found online at https://doi.org/10.1016/j.sab.2022.106399.

References

[1] K. Gschneider, J.-C. Bünzli, V. Pecharsky, Handbook on the Physics and Chemistry of Rare Earths 1st ed, vol. 4, Elsevier, 2004.

[2] C.P. Balde, E-Waste Monitor, 2014, https://doi.org/10.1007/s00705-012-1479-4.

[3] B. Achzet, A. Reller, C. Rennie, M. Ashfield, J. Simmons, Materials Critical to the Energy Industry. An Introduction, University of Augsburg, ON Commun, 2011.

[4] J.H. Rademaker, R. Kleijn, Y. Yang, Recycling as a strategy against rare earth element criticality: a systemic evaluation of the potential yield of NdFeB magnet recycling, Environ. Sci. Technol. 47 (2013) 10129–10136, https://doi.org/10.1021/es305007w.

[5] E. Alonso, A.M. Sherman, T.J. Wallington, M.P. Everson, F.R. Field, R. Roth, et al., Evaluating rare earth element availability: a case with revolutionary demand from clean technologies, Environ. Sci. Technol. 46 (2012) 3406–3414, https://doi.org/10.1021/es203518d.

[6] B. Zhou, Z. Li, C. Chen, Global potential of rare earth resources and rare earth demand from clean technologies, Minerals. 7 (2017) 203, https://doi.org/10.3390/min7110203.

[7] Q. Tan, C. Deng, J. Li, Innovative application of mechanical activation for rare earth elements recovering: process optimization and mechanism exploration, Sci. Rep. 6 (2016) 19961, https://doi.org/10.1038/srep19961.

[8] Q. Tan, J. Li, X. Zeng, Rare earth elements recovery from waste fluorescent lamps: a review, Crit. Rev. Environ. Sci. Technol. 45 (2015) 749–776, https://doi.org/10.1080/10643389.2014.900240.

[9] A.B. Patil, R.P.W.J. Struis, A.J. Schuler, M. Tarik, A. Krebs, W. Larsen, et al., Rare earth metals recycling from E-wastes: strategy and perspective, in: C. Ludwig, S. Valdivia (Eds.), Prog. Towar. Resour. Revolut., World Resources Forum, Villligen PSI and St. Gallen, 2019, pp. 162–164.

[10] D. Dupont, K. Binnemans, Recycling of rare earths from NdFeB magnets using a combined leaching/extraction system based on the acidity and thermomorphism of

the ionic liquid [Hbet][Tf$_2$N], Green Chem. 17 (2015) 2150–2163, https://doi.org/10.1039/c5gc00155b.

[11] D. Dupont, K. Binnemans, Rare-earth recycling using a functionalized ionic liquid for the selective dissolution and revalorization of Y$_2$O$_3$:Eu^{3+} from lamp phosphor waste, Green Chem. 17 (2015) 856–868, https://doi.org/10.1039/C4GC02107J.

[12] D. Kim, L. Powell, L.H. Delmau, E.S. Peterson, J. Herchenroeder, R.R. Bhave, A supported liquid membrane system for the selective recovery of rare earth elements from neodymium-based permanent magnets, Sep. Sci. Technol. 51 (2016) 1716–1726, https://doi.org/10.1080/01496395.2016.1171782.

[13] X. Yin, Y. Wang, X. Bai, Y. Wang, L. Chen, C. Xiao, et al., Rare earth separations by selective borate crystallization, Nat. Commun. 8 (2017) 14438, https://doi.org/10.1038/ncomms14438.

[14] C. Tunsu, J.B. Lapp, C. Ekberg, T. Retegan, Selective separation of yttrium and europium using Cyanex 572 for applications in fluorescent lamp waste processing, Hydrometallurgy. 166 (2016) 98–106, https://doi.org/10.1016/j.hydromet.2016.10.012.

[15] C. Tunsu, C. Ekberg, T. Retegan, Characterization and leaching of real fluorescent lamp waste for the recovery of rare earth metals and mercury, Hydrometallurgy. 144–145 (2014) 91–98, https://doi.org/10.1016/j.hydromet.2014.01.019.

[16] M.K. Jha, A. Kumari, R. Panda, J. Rajesh Kumar, K. Yoo, J.Y. Lee, Review on hydrometallurgical recovery of rare earth metals, Hydrometallurgy. 165 (2016) 2–26, https://doi.org/10.1016/j.hydromet.2016.01.035.

[17] S. Van Loy, K. Binnemans, T. Van Gerven, Recycling of rare earths from lamp phosphor waste: Enhanced dissolution of LaPO$_4$:Ce^{3+},Tb^{3+} by mechanical activation, J. Clean. Prod. 156 (2017) 226–234, https://doi.org/10.1016/j.jclepro.2017.03.160.

[18] P. Venkatesan, T. Vander Hoogerstraete, K. Binnemans, Z. Sun, J. Sietsma, Y. Yang, Selective extraction of rare-earth elements from NdFeB magnets by a room-temperature electrolysis pretreatment step, ACS Sustain. Chem. Eng. 6 (2018) 9375–9382, https://doi.org/10.1021/acssuschemeng.8b01707.

[19] A.B. Patil, M. Tarik, R.P.W.J. Struis, C. Ludwig, Exploiting end-of-life lamps fluorescent powder e-waste as a secondary resource for critical rare earth metals, Resour. Conserv. Recycl. 164 (2021) 105153, https://doi.org/10.1016/j.resconrec.2020.105153.

[20] Y. Wu, X. Yin, Q. Zhang, W. Wang, X. Mu, The recycling of rare earths from waste tricolor phosphors in fluorescent lamps: a review of processes and technologies, Resour. Conserv. Recycl. 88 (2014) 21–31, https://doi.org/10.1016/j.resconrec.2014.04.007.

[21] B. Zawisza, K. Pytlakowska, B. Feist, M. Polowniak, A. Kita, R. Sitko, Determination of rare earth elements by spectroscopic techniques: a review, J. Anal. At. Spectrom. 26 (2011) 2373–2390, https://doi.org/10.1039/c1ja10140d.

[22] N.H. Bings, A. Bogaerts, J.A.C. Broekaert, Atomic spectroscopy: a review, Anal. Chem. 82 (2010) 4653–4681, https://doi.org/10.1021/ac1010469.

[23] A.B. Patil, A.J. Schuler, R.P.W.J. Struis, C. Ludwig, World INtellectual Property Buro, WO2019/201582A1, 2019 p. WO2019/201582A1.

[24] S.P. Verma, E. Santoyo, F. Velasco-Tapia, Statistical evaluation of analytical methods for the determination of rare-earth elements in geological materials and implications for detection limits, Int. Geol. Rev. 44 (2002) 287–335, https://doi.org/10.2747/0020-6814.44.4.287.

[25] K. Kawabata, Y. Kishi, O. Kawaguchi, Y. Watanabe, Y. Inoue, Determination of rare-earth elements by inductively coupled plasma mass spectrometry with ion chromatography, Anal. Chem. 63 (1991) 2137–2140, https://doi.org/10.1021/ac00019a013.

[26] E. Blanchard, A. Nonell, F. Chartier, A. Rincel, C. Bresson, Evaluation of superficially and fully porous particles for HILIC separation of lanthanide-polyaminocarboxylic species and simultaneous coupling to ESIMS and ICPMS, RSC Adv. 8 (2018) 24760–24772, https://doi.org/10.1039/c8ra02961j.

[27] K.G. Myhre, M.J. Mehta, M.Z. Martin, M. Du, Laser induced breakdown spectroscopy analysis of europium and samarium in aluminum oxide, Spectrochim. Acta - Part B At. Spectrosc. 149 (2018) 30–34, https://doi.org/10.1016/j.sab.2018.07.014.

[28] I. Wysocka, E. Vassileva, Method validation for high resolution sector field inductively coupled plasma mass spectrometry determination of the emerging contaminants in the open ocean: rare earth elements as a case study, Spectrochim. Acta - Part B At. Spectrosc. 128 (2017) 1–10, https://doi.org/10.1016/j.sab.2016.12.004.

[29] Y. Fujita, J. Barnes, A. Eslamimanesh, M.M. Lencka, A. Anderko, R.E. Riman, et al., Effects of simulated rare earth recycling wastewaters on biological nitrification, Environ. Sci. Technol. 49 (2015) 9460–9468, https://doi.org/10.1021/acs.est.5b01753.

[30] J. Knoop, U. Oppermann, J. Scharm, Interference-free determination of REEs in electronic waste using ICP optical emission spectroscopy, J. Chem. Chem. Eng. 8 (2014) 635–640.

[31] A. Sengupta, Y. Airan, S.K. Thulasidas, V. Natarajan, Appraising the spectral interference of dysprosium on 27 analytes using capacitively coupled device detector-based inductively coupled plasma atomic emission spectrometry without physical/chemical separation, At. Spectrosc. 37 (2016) 50–60, https://doi.org/10.46770/as.2016.02.003.

[32] P.W.J.M. Boumans, H. Zhizhuang, J.J.A.M. Vrakking, J.A. Tielrooy, F.J.M.J. Maessen, Mutual spectral interferences of rare earth elements in inductively coupled plasma atomic emission spectrometry-III. Pseudo physically resolved spectral data: complete results and evaluation, Spectrochim. Acta Part B At. Spectrosc. 44 (1989) 31–93, https://doi.org/10.1016/0584-8547(89)80146-6.

[33] P.W.J.M. Boumans, J.A. Tielrooy, F.J.M.J. Maessen, Mutual spectral interferences of rare earth elements in inductively coupled plasma atomic emission spectrometry. I. Rational line selection and correction procedure, Spectrochim.

Acta Part B At. Spectrosc. 43 (1988) 173–199, https://doi.org/10.1016/0584-8547(88)80006-5.

[34] N. Daskalova, S. Velichkov, P. Slavova, Spectral interferences in the determination of traces of scandium, yttrium and rare earth elements in "pure" rare earth matrices by inductively coupled plasma atomic emission spectrometry Part III, Europium, Spectrochim. Acta - Part B At. Spectrosc. 51 (1996) 733–768, https://doi.org/10.1016/0584-8547(96)01472-3.

[35] P.W.J.M. Boumans, Some recent studies of inductively coupled plasmas involving the measurement or use of physical line widths: a tutorial discussion with retrospects and extensions, Spectrochim. Acta Part B At. Spectrosc. 44 (1989) 1325–1344, https://doi.org/10.1016/0584-8547(89)80128-4.

[36] L.L. Burton, M.W. Blades, Computer simulation of spectral interferences in inductively coupled plasma-optical emission spectroscopy, Spectrochim. Acta Part B At. Spectrosc. 43 (1988) 305–315, https://doi.org/10.1016/0584-8547(88)80060-0.

[37] J. Chappell, M. Martinez, M. Baudelet, Statistical evaluation of spectral interferences in laser-induced breakdown spectroscopy, Spectrochim, Acta - Part B At. Spectrosc. 149 (2018) 167–175, https://doi.org/10.1016/j.sab.2018.07.028.

[38] D. Wienke, C. Lucasius, G. Kateman, Multicriteria target vector optimization of analytical procedures using a genetic algorithm. Part I. Theory, numerical simulations and application to atomic emission spectroscopy, Anal. Chim. Acta 265 (1992) 211–225, https://doi.org/10.1016/0003-2670(92)85027-4.

[39] A.S. Al-Ammar, R.K. Gupta, R.M. Barnes, Correction for non-spectroscopic matrix effects in inductively coupled plasma-mass spectrometry by common analyte internal standardization, Spectrochim. Acta - Part B At. Spectrosc. 54 (1999) 1849–1860, https://doi.org/10.1016/S0584-8547(99)00129-9.

[40] K.P. Li, J.D. Hwang, J.D. Winefordner, Studies of chemical interferences in an inductively coupled plasma using moment analysis of space-resolved emission profiles, Anal. Chem. 62 (1990) 1233–1238, https://doi.org/10.1021/ac00212a008.

[41] A.B. Patil, V.S. Shinde, P. Pathak, P.K. Mohapatra, New extractant N,N′-dimethyl-N,N′-dicyclohexyl-2,(2′-dodecyloxyethyl)-malonamide (DMDCDDEMA) for radiotoxic acidic waste remediation: synthesis, extraction and supported liquid membrane transport studies, Sep. Purif. Technol. 145 (2015) 83–91, https://doi.org/10.1016/j.seppur.2015.02.041.

[42] Advanced Magnets For Greener & Smarter Future. www.advancedmagnets.com/introduction-to-basic-composition-and-microstructure-of-sintered-ndfeb-magnet/ (accessed August 8, 2021).